J. Am. Soc. Mass Spectrom. (2019) 30:299–308
DOI: 10.1007/s13361-018-2081-0

RESEARCH ARTICLE

# Sputter-Coated Metal Screening for Small Molecule Analysis and High-Spatial Resolution Imaging in Laser Desorption Ionization Mass Spectrometry

Rebecca L. Hansen, Maria Emilia Dueñas, Young Jin Lee

Department of Chemistry, Iowa State University, Ames, IA 50011, USA

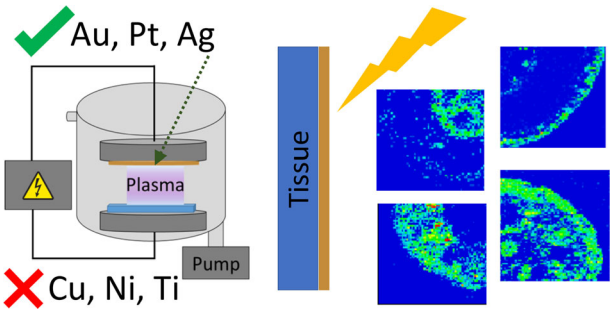


**Abstract.** Nanoparticles are efficient matrices in laser desorption/ionization (LDI) mass spectrometry (MS), especially for the profiling or imaging of small molecules. Recently, solvent-free physical vapor desorption (PVD), or sputter coating, was adopted as a homogenous method to rapidly apply metal nanoparticles (NPs) in situ to samples prior to LDI MS or MS imaging analysis. However, there has been no systematic study comparing different metal targets for the analysis of a variety of small molecule metabolites. Here, we present a screening and optimization of various sputter-coated metals, including Ag, Au, Cu, Pt, Ni, and Ti, for LDI analysis of small molecules in both positive and negative ion modes. Optimized sputter coating is then applied to high-spatial resolution LDI mass spectrometry imaging (MSI) of maize root and seed cross-sections. Noble metals, Ag, Au, and Pt, are found to be much more efficient than transition metals and organic matrices for most small metabolites. Sputter-coated metals are efficient for neutral lipids, such as triacylglycerols and diacylglycerols, but are very inefficient for most phospholipids.

**Keywords:** Sputter coating, Laser desorption ionization, Mass spectrometry imaging, Nanoparticles, Noble metals, Small molecule imaging

Received: 5 July 2018/Revised: 30 September 2018/Accepted: 2 October 2018/Published Online: 19 October 2018

## Introduction

Various types of nanoparticles (NPs), especially carbon-based NPs and metal oxide NPs, have been reported to be efficient matrices for laser desorption/ionization mass spectrometry (LDI-MS) analysis for a variety of applications [1–4]. NPs have no or low matrix background, and are therefore particularly useful for the analysis of low molecular weight compounds. This is in contrast to traditional organic matrices which display high matrix background that can interfere with small molecule analysis. Other advantages of NPs include high laser absorptivity in the UV range, non-volatility—thus are stable in vacuum conditions for MS imaging experiments—and no "hot spot" formation issues as they can be homogenously applied.

Previously, we have performed a large-scale screening of 13 different NPs, including three carbon-based NPs, six metal oxide NPs, and four metal NP suspensions, for the analysis of two dozen small metabolites that represent a wide variety of classes of compounds [5]. We found that although metal NP suspensions did show some success as matrices, their tendency to aggregate in solution greatly limited their suitability as matrices. This aggregation was especially apparent and rapid for platinum and gold, and to a lesser extent for copper and silver [5]. Capping agents (e.g., citrate) are commonly used in nanoparticle synthesis to control the size of NPs and improve NP stability. NPs capped with organic compounds have been previously utilized in LDI-MS, especially for macromolecule analyses [6–8]. For small molecule analysis, however, the release of organic capping agents in LDI analyses often results in ion suppression, thus minimizing their practicality as small molecule matrices [9, 10]. Some capping agents have been

**Electronic supplementary material** The online version of this article (https://doi.org/10.1007/s13361-018-2081-0) contains supplementary material, which is available to authorized users.

*Correspondence to:* Young Lee; *e-mail:* yjlee@iastate.edu

successfully used in LDI-MS of small molecules though, such as glutathione-capped iron oxide NPs for glycans [11].

Physical vapor deposition (PVD), or sputter coating, has been reported to be an efficient means to create metal nanoparticles in situ [12–16]. Sputter coating allows metal NPs to be rapidly and homogenously deposited onto samples in nanometer thin layers, and thus eliminates the aggregation problem in metal NP suspensions. Although several studies have used sputter coating to apply metal matrices for LDI analysis, these studies have focused solely on one metal for a particular class of compounds. For example, sputtered Au has been used to analyze neurotransmitters and fatty acids in mice tumors [12], Na-doped Au to detect triacylglycerols (TAGs) on tissue [14], Ag to visualize cholesterol in human fibroblasts [15] as well as olefins in mice and rat tissues [13], and Pt combined with 2,5-dihydroxybenzoic acid as a matrix for phosphocholine (PC) and phosphoethanolamine (PE) in rat brain tissue [16]. To date, no effort has been made to systematically compare multiple metals for the analysis of a variety of classes of small metabolites.

In this work, six metals, gold (Au), silver (Ag), copper (Cu), platinum (Pt), nickel (Ni), and titanium (Ti), are tested for their efficiency as matrices for LDI analysis of small molecules when deposited via sputter coating. Firstly, the metals are optimized and applied to the analysis of a water-soluble and a water-insoluble standard mixture of compounds. Once the experimental conditions are optimized, these six metals are applied to the LDI mass spectrometry imaging (MSI) analysis of maize root and seed cross-sections, in both positive and negative ion mode.

## Experimental

### *Materials*

Metal sputtering targets, gold (99.99% Au), silver (99.99% Ag), copper (99.99% Cu), platinum (99.95% Pt), nickel (99.98% Ni), and titanium (99.6%) were purchased from Ted Pella, Inc. (Redding, CA, USA). 2,5-Dihydroxybenzoic acid (DHB, 98.0%) and 1,5-diaminonaphthalene (DAN, 97.0%) were purchased from Sigma Aldrich (St. Louis, MO, USA). The metabolite standard malic acid, glucose, glucose-6-phosphate, sucrose, asparagine, glutamic acid, isoleucine, biotin (vitamin H), glycerol tripalmitate, vanillic acid, and oleic acid were purchased from Sigma Aldrich (St. Louis, MO, USA). Ascorbic acid was purchased from Fisher Scientific (Hampton, NH, USA). Phosphoenolpyruvic acid monopotassium salt was purchased from Alfa-Aesar (Ward Hill, MA, USA). Rac-glycerol 1-phosphate disodium salt hexahydrate was purchased from Santa Cruz Biotechnology, Inc. (Dallas, TX, USA). Phosphocholine chloride sodium salt hydrate was purchased from Tokyo Chemical Industry Co. Ltd. (Philadelphia, PA, USA). Parthenolide was purchased from TORIS Bioscience (Bristol, UK). Phospholipid mixture [L-α-phosphatidylcholine, 20% (Soy) (Soy Total Lipid Extract)] was purchased from Avanti Polar Lipids, Inc. (Alabaster, AL, USA). Chloroform (Certified ACS) and water (Optima LC/MS) were purchased from Fisher Scientific (Hampton, NH, USA). Isopropanol (LCMS Chromasolv®) was purchased from Sigma Aldrich (St. Louis, MO, USA). μFocus MALDI plates (90 circles, 600 μm) were purchased from Hudson Surface Technology (Old Tappan, NJ, USA). Gelatin from porcine skin (300 bloom) was purchased from Electron Microscopy Sciences (Hatfield, PA, USA). B73 inbred corn seeds were obtained from Dr. Marna Yandeau-Nelson at Iowa State University.

### *Preparation of Metabolite Standards*

Two sets of standard solutions, water-soluble and water-insoluble, were prepared in either water or chloroform, respectively at 1 mM for each analyte. The water-soluble standard mixture includes malic acid, vanillic acid, ascorbic acid, phosphoenolpyruvic acid, glycerol-3-phosphate, phosphocholine, glucose, sucrose, glucose-6-phosphate, glutamic acid, isoleucine, asparagine, and vitamin H. The water-insoluble standard mixture includes glycerol tripalmitate, oleic acid, parthenolide, and assorted phospholipids (soy lipid phospholipid mixture). For the phospholipid mixture, an average molecular weight of 1000 g $mol^{-1}$ was used to calculate concentration, as it contains a mixture of lipid species. The standards were diluted 1:10 in isopropanol for a final concentration of 100 μM for each standard. Each standard solution was spotted (2 μL) onto a μFocus MALDI plate pre-heated to 35 °C to ensure uniform deposition. For comparison of sputtered metals to organic matrices, 10 mM DHB and DAN were prepared in isopropanol for positive and negative mode, respectively. After the standard solution was spotted and allowed to dry, 2 μL of organic matrix was spotted.

### *Preparation of Maize Root and Seed*

A B73 inbred corn seed was imbibed by shaking it for 10 min at 300 rpm in a glass scintillation vial with deionized water. Using a razor blade, the seed was cut longitudinally approximately halfway between the edge and center. The seed was then immediately flash frozen in liquid nitrogen to prevent metabolite turnover. Once frozen, the seed was placed, cut-side down, into a cryo-mold which was then filled with a 10% *w*/*v* gelatin solution, and then immediately frozen with liquid nitrogen.

To prepare root cross-section samples, B73 inbred corn seeds were grown using a previously described method [17]. Briefly, a row of seeds, embryo facing down, were staggered along the top edge of a moist brown paper towel. The paper towel was then rolled tightly enough to hold the seeds in place and the bottom of the roll was placed into a 1-L beaker filled halfway with water. The seeds were grown for 11 days in the dark, and periodically monitored to ensure water covered the lower portion of the paper towel roll. The roots were harvested when the lengths of the primary root was approximately 10–14 cm, as measured from the tip of the root. The area of interest, approximately 2 cm from the seed, was embedded in a cryo-mold filled with 10% *w*/*v* gelatin solution, and flash-frozen in liquid nitrogen.

In either the case of seeds or roots, the mold containing the sample was floated on liquid nitrogen until the gelatin was mostly opaque. Molds were transferred to a cryostat (CM1850; Leica Microsystems, Buffalo Grove, IL, USA) pre-chilled to – 22 °C. Once thermally equilibrated, the gelatin block was mounted onto a cryostat chuck and sectioned at 10 μm thickness. The sections were captured using adhesive tape windows (Leica Biosystems, Buffalo Grove, IL, USA), and then taped to pre-chilled glass slides. Samples were stored at – 80 °C until needed. Before analysis, the slides were lyophilized under vacuum followed by metal matrix application.

### *Metal Sputter Coating*

Metals were selected based on studies involving nanoparticle suspensions [5], preliminary unpublished experiments, and literature results. Metals were applied to either spotted standard samples or tissue sections using a sputter coater instrument from Ted Pella, Inc. (Cressington 108Auto; Redding, CA, USA). A MTM-20 High Resolution Thickness Controller (Ted Pella) was used to monitor and/or control the deposited metal layer thickness. The distance between the metal target and the sample was ~ 4 cm during sputtering. The chamber was flushed with argon gas (pressure ~ 8 psi) twice before sputter coating. The sputtering current was tested at 20 and 40 mA; however, minor differences were noted and so 40 mA was selected for all tests and analyses. Sputtering time was individually optimized for each metal nanoparticle.

Various sputtering times were compared for each metal in both positive and negative ion mode. The testing range for each metal was selected based on reported optimal sputtering times in the literature and our own preliminary tests. The sputtering times tested were 2, 5, 10, 15, 20, 30, and 40 s for gold and silver; and 5, 10, 20, 30, 40, 50, and 60 s for platinum, titanium, copper, and nickel. Absolute ion intensities for the metabolite standards were compared across 3–4 replicates with each standard mixture and ion mode to determine the optimal sputtering times. These times were then used in the MSI analysis of the maize roots and seeds.

### *Mass Spectrometric Data Acquisition*

Data was acquired using a MALDI-linear ion trap (LIT)-Orbitrap mass spectrometer (MALDI-LTQ-Orbitrap Discovery; Thermo Finnigan, San Jose, CA, USA) with an external frequency-tripled Nd:YAG laser operating at 355 nm and 60 Hz (UVFQ; Elforlight Ltd., Daventry, UK). The laser energy was optimized individually for each matrix (Supplemental Table 1) and 10 laser shots were used to acquire each spectrum. The Orbitrap mass analyzer (resolution 30,000 at *m/z* 400) was used to acquire all standard and maize root imaging data for a *m/z* range of 50–1000 in both positive and negative ion modes. Corn seed images were analyzed using 20 laser shots per spectrum and using a mass range of *m/z* 300–1000 to target lipid species in both ion modes. Maize root images were acquired using 10 μm raster steps (laser spot size of 9 μm) and seed images using 100 μm raster steps (laser spot size of 50 μm). MS/MS spectra were manually collected using individually optimized collision energies.

All MS images shown were generated using ImageQuest (Thermo) with a ± 0.01 Da mass tolerance and normalization to the total ion count. The maximum and minimum values used to generate MS images were arbitrarily adjusted for each molecular species to obtain the best visualization. The same values were used for all matrices with a particular molecular species to facilitate comparisons. Peak assignments were made using accurate mass searches on the Metlin database (https://metlin.scripps.edu) [18] as well as manual MS/MS analysis and in silico fragmentation using CFM-ID (http://cfmid.wishartlab.com/) [19].

### *AFM Measurements*

Samples were prepared by placing a coverslip onto a clean glass slide (to serve as a control or background area). Each metal was sputtered onto a separate glass slide for the optimal deposition time. Before analysis, a clean needle was used to make several scratches in the sputtered metal surface, to produce a clear area for analysis. The atomic force microscope (AFM) images were captured in SCAN Assist mode on a Dimension ICON AFM (Bruker Nano Surfaces, Santa Barbara, CA, USA). All AFM images were captured in air and were processed to remove sample tilt. Thickness measurement data was collected using the Nanoscope software by calculating the height difference between two areas of an AFM image. The areas selected were observed as either representative of the coating or the background substrate and the average difference between these areas was reported as the thickness of the coating.

## Results and Discussion

### *Sputtering Time Optimization*

Firstly, the six different metals are applied to the analysis of a water-soluble and a water-insoluble standard mixture of compounds which includes small organic acids, sugars, phosphate-containing metabolites, amino acids, a vitamin, glycerolipid species, a fatty acid, and a terpene for both ion modes. The sputtering conditions, including sputtering time and sputtering current, are optimized individually for each metal matrix. The analysis with standard mixtures establishes which types of metabolites are effectively desorbed/ionized by each metal matrix. Prior to sputtering time optimization, the optimal laser energy for each matrix was determined using the water-soluble standard mixture. Data was collected by increasing the laser energy in step-wise fashion over the typical laser energy settings for our instrument. Once the optimum laser energy was established for each metal matrix, this laser energy was used for all other data collection (Supplemental Table 1).

To optimize sputtering times (corresponding to deposited thicknesses) for each metal, mixtures of water-soluble and

water-insoluble standards were analyzed in both positive and negative ion mode. The two sets of standard samples were analyzed in triplicate using the laser energy that was optimized for each metal matrix. Each standard mixture was spotted onto a MALDI microarray plate, and then metals were sputter deposited for the selected set of times. In positive ion mode, most metabolite standards were detected as alkali metal adducts ($[M+Na]^+$ and $[M+K]^+$), but also as protonated species ($[M+H]^+$), and silver adducts ($[M+Ag]^+$) with the silver metal matrix. In negative mode, metabolite standards were detected as both deprotonated $[M-H]^-$ and water loss $[M-H_2O-H]^-$ species. To compare between different matrices, ion signals were summed over the multiple adducts for each standard compound.

The screening results for all six metals using water-soluble metabolite standards in positive and negative ion mode at all tested deposition times are presented in Supplemental Table 2. The darkest color in a given column (i.e., for a particular metabolite) indicates a higher ion signal for that compound relative to other sputtering times. In many of the cases, the dark coloring is quite apparently clustered at one particular time, for example, 10 s for Au in positive and negative ion modes. However, for Ni, especially in positive mode, the best time varied quite significantly across the metabolites, likely due to the overall very low signal intensity, and so the middle value, 30 s, was chosen for further studies. The optimal sputtering times were determined to be as follows: 5–10 s for Ag, 10 s for Au, 30 s for Ni, 10 s for Pt, and 30 s for Ti in both ion modes. Cu displayed significant differences between the two ion modes, and so 60 s was selected for positive ion mode and 5–10 s for negative mode. Longer deposition times of 70 and 80 s for Cu were also tested in positive mode (data not shown), but resulted in decreased signal intensities compared to 60 s. In the case of Ag, ion signals between 5 and 10 s were highly comparable, mostly within 10% difference; 10 s is slightly better in positive mode and 5 s is slightly better in negative mode. We have arbitrarily chosen 5 s for the subsequent tissue applications. It is important to note that a slight deviation from the optimal time will not result in huge signal changes for the majority of the metabolites tested. Additionally, minimal or no differences in optimal sputtering times were found between water-soluble and water-insoluble standards. Measured thicknesses for the optimal sputtering times are reported using both a MTM-20 High Resolution Thickness Controller (Ted Pella, Inc.) and a Dimension ICON Atomic Force Microscope (AFM) (Bruker Nano Surfaces) in Supplemental Table 3. Overall, the AFM measurements are about three times thicker than those reported using the MTM-20 Thickness Controller.

Thicker metal layers have been reported by some groups, for example, 28 ± 3 nm Au for TAG analysis [14] compared to 9.3 nm in our experiments. However, higher thicknesses resulted in signal loss in our instrument setup. In support of our results indicating thinner metal layers are optimal, Li et al. did report 2 nm water-soluble Au nanoclusters to be more efficient compared to 20 nm Au nanoparticles for a variety of small molecules [20]. Additionally, Ozawa et al. reported 3.0 nm as the optimal sputtered Pt thickness [16] and Tang et al. determined 4 nm of sputtered Au to be ideal [12]. It is important to note that the optimal condition might be slightly different depending on the target metabolites or tissue types. For example, Dufresne et al. optimized directly on-tissue for TAG species and determined the most optimal Au thickness as 28 ± 3 nm [14]. In this study, multiple classes of compounds were considered and the optimum condition was chosen based on the overall trend for the majority of metabolites. The goal of this work is to compare the relative efficiencies of the metal matrices for various classes of metabolites and to provide a guideline for use of metal matrices in small molecule analysis.

## *Comparison of Optimized Matrices Using Standards*

The six metal thin films are compared in Fig. 1 for their efficiency as LDI matrices in analyzing water-soluble and

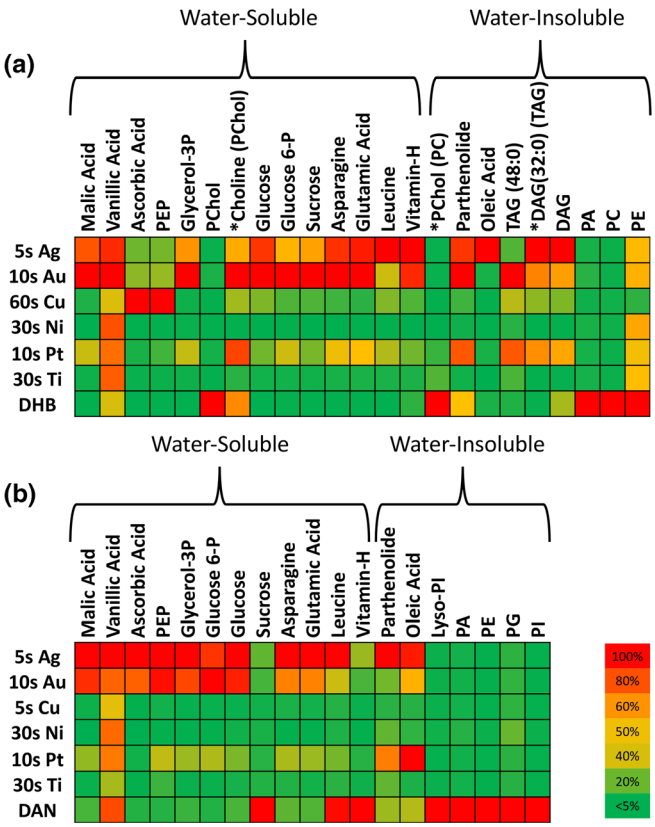


**Figure 1.** Summary of sputter-coated metal screening for small metabolite analysis in (**a**) positive and (**b**) negative ion mode. Ion signals are normalized to the highest ion signal for each analyte and shown as a heatmap with the color scale shown as a percentage of the maximum. An asterisk indicates a fragment ion with the precursor shown in parentheses. PEP, phosphoenolpyruvic acid; Glycerol-3P, glycerol-3-phosphate; PChol, phosphocholine; Glucose 6-P, glucose 6-phosphate; PC, phosphocholine; TAG, triacylglycerol; DAG, diacylglycerol; PA, phosphatidic acid; PE, phosphatidylethanolamine; PI phosphatidylinositol; PG, phosphatidylglycerol; DHB, 2,5-dihydroxybenzoic acid; DAN, 1,5-diaminonaphthalene

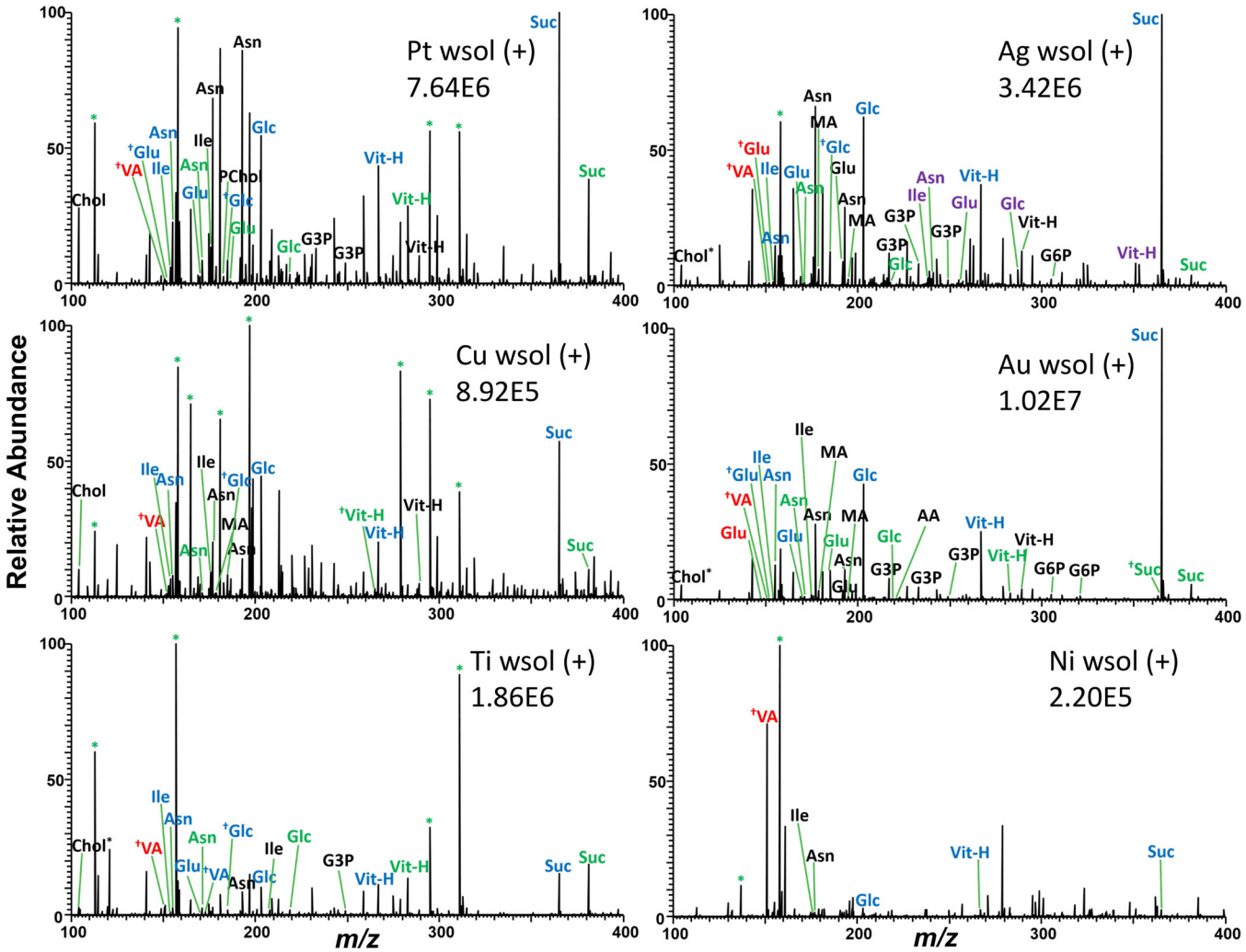


**Figure 2.** Representative mass spectra for each metal matrix at the optimal sputtering time for the water-soluble standard mixture in positive ion mode. MA, malic acid; VA, vanillic acid; AA, ascorbic acid; PEP, phosphoenolpyruvic acid; G-3P, glycerol-3-phosphate; PChol, phosphocholine; Chol, choline; Glc, glucose; Glc 6-P, glucose 6-phosphate; Suc, sucrose; Asn, asparagine; Glu, glutamic acid; Leu, leucine/isoleucine; Vit-H, biotin (vitamin H). Color coding is used to indicate various adduct types as follows: red = proton adducts, blue = sodium adducts, green = potassium adducts, purple = silver adducts, black = di-alkali metal adducts. Dagger sign indicates a water loss. Note that choline is detected as a molecular ion

water-insoluble analytes at each optimized condition. In terms of overall signal intensity across the broad range of metabolites studied, Au and Ag were almost equally effective. Ion signals for each metabolite with each matrix are presented in Supplemental Table 4. Representative mass spectra for each metal matrix in each ion mode with each standard mixture are presented in Fig. 2 (water-soluble standards in positive mode) and Supplemental Figure 1 (water-soluble standards in negative mode and water-insoluble standards in positive and negative mode). Peaks that correspond to a standard compound are indicated on each spectrum with the base ion intensity for each spectrum indicated in the upper right corner.

Although both Au and Ag are highly efficient in both ion modes, in positive mode, Au is slightly better for sugar-containing metabolites, but in negative mode, Ag is slightly more effective for amino acids. In positive ion mode, Ag does create adducts with metabolites, increasing sample complexity, and silver clusters are present in the spectrum at moderate abundance. While Au and Ag were the most efficient of the matrices tested, Pt also displayed good signal intensity, only moderately lower than Au and Ag, for the majority of the metabolites, and was almost equally effective for some metabolites including parthenolide, a terpene which is a particularly problematic class of compounds to analyze in MALDI [21], and oleic acid. Copper showed poor performance for most metabolites, but produced decent ion signals for selected metabolites, including higher signal intensity for ascorbic acid and phosphoenolpyruvic acid in positive ion mode compared to Au or Ag. Ni and Ti generally showed the lowest ion signal of the six metal matrices; however, they still provide sufficient signal for some analytes, such as vanillic acid, glutamic acid, and sugars, although the absolute intensities are lower than with Au, Ag, or Pt.

In addition to the metal matrices being compared to themselves, they were also compared to traditional organic matrices

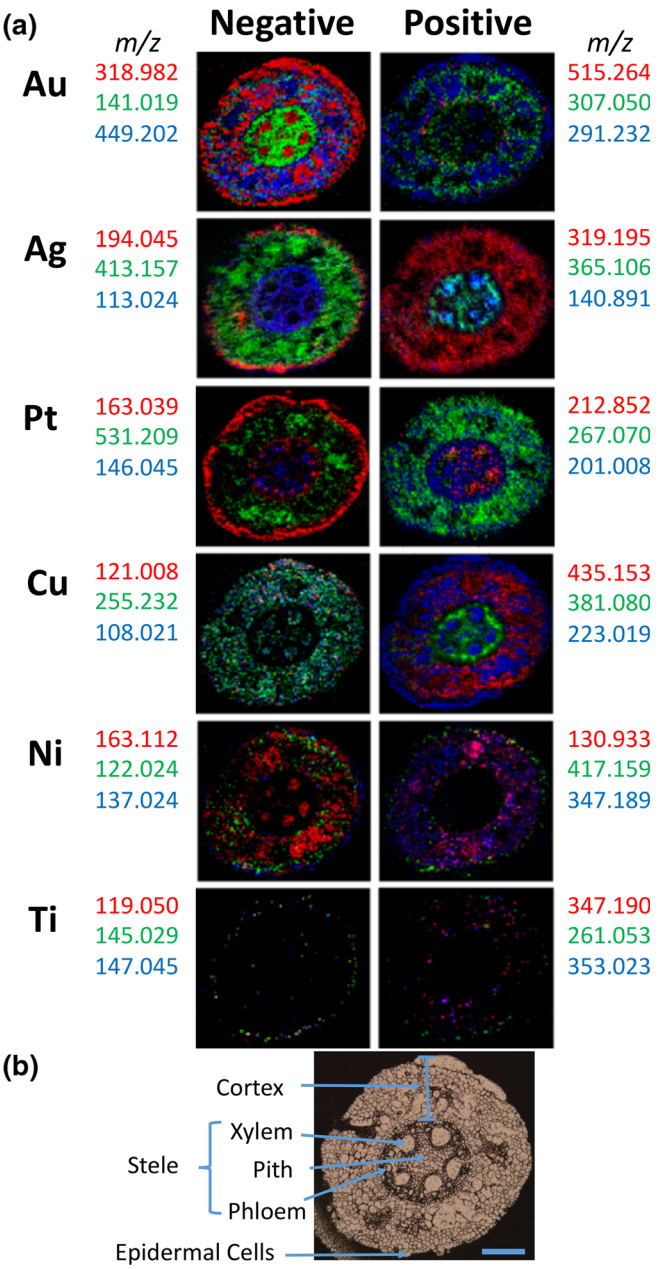


**Figure 3.** (**a**) Representative MALDI MS images of B73 maize root cross-sections showing localizations of various metabolites with each metal matrix. (**b**) Morphology of maize root. Scale bar 200 μm. See Supplemental Table 5 for identifications

(Fig. 1). Compared to DHB, a common organic matrix for positive mode, Au and Ag are more effective for most metabolites tested. However, DHB was the only matrix that produced good ion signals for phospholipids in positive mode (i.e., PA, PC, and PE) (Fig. 1a). In negative mode, the metal matrices were compared to DAN, a common organic matrix for negative mode. DAN was more effective for certain metabolites, such as vitamin H and phospholipids, but Au and Ag were more effective for many of the metabolites including phosphoenolpyruvic acid, glucose-containing metabolites, parthenolide, and oleic acid (Fig. 1b).

Overall, this study demonstrates that Ag and Au are generally more effective than organic matrices in both ion modes for most compounds. In positive mode, this is similar to our previous report where many nanoparticle matrices, including $TiO_2$, $Fe_3O_4$, and boron-doped nano-diamond (BDND), are overall more effective than organic matrices [5]. Previously in negative mode, DAN was discovered to be much more effective for small molecule metabolites compared to any of the NP suspensions [5], whereas the current study demonstrates that sputter-coated metal nanoparticles are generally better than DAN in negative mode. Despite the effectiveness of metal matrices compared to the organic matrices, none of the six metal matrices were effective for phospholipid species, although they were effective for some small phosphate-containing species such as glycerol-3-phosphate (Fig. 1). This is an interesting phenomenon but we could not find any good answer at this point. In contrast, DHB and DAN were effective for phospholipid species in both ion modes. Pt, Ag, and Au, however, were all effective for neutral lipid species in positive mode, such as triacylglycerols (TAGs) and diacylglycerol (DAGs), whereas DHB was less effective. Dufresne et al. also previously found TAGs to be effectively desorbed/ionized using sodium-doped sputtered Au on mouse liver tissues [14].

Interestingly, in most cases with the metal matrices, there was not a prominent matrix-dependent analyte selectivity, which is commonly known for organic matrices and has also been shown for carbon-based nanoparticles [21]. The one major exception to this, as previously discussed, is phospholipid species that were not effectively desorbed/ionized by any of the six metal matrices in either positive or negative ion mode, although they were using the organic matrices. Most of the other classes of compounds tested in this study were effectively analyzed by the noble metals, Ag and Au, followed by Pt. We hypothesize the non-selectivity of the noble metals might be due to the high reduction potential and/or low reactivity of these metals.

## *Comparison of Au Deposition Time On-Tissue*

In consideration of reports indicating higher Au thicknesses were optimal for on-tissue analysis [12, 14], consecutive tissue sections were analyzed with either 10 s or 40 s sputtered Au. In general, for maize tissues analyzed in our instrument setup, 10 s produced higher quality images and greater signal intensities in the low mass region of *m/z* 50–500. Representative images for selected metabolites are shown in Supplemental Figure 2. Images are normalized to the TIC and have the same maximum and minimum values for each metabolite to facilitate comparison; the same trend is found when compared without normalization. For example, hexose and di-hexose are clearly imaged with 10 s Au, but minimal signal intensity is present when a consecutive tissue section is imaged using 40 s Au. These results were repeated using a different root with similar results.

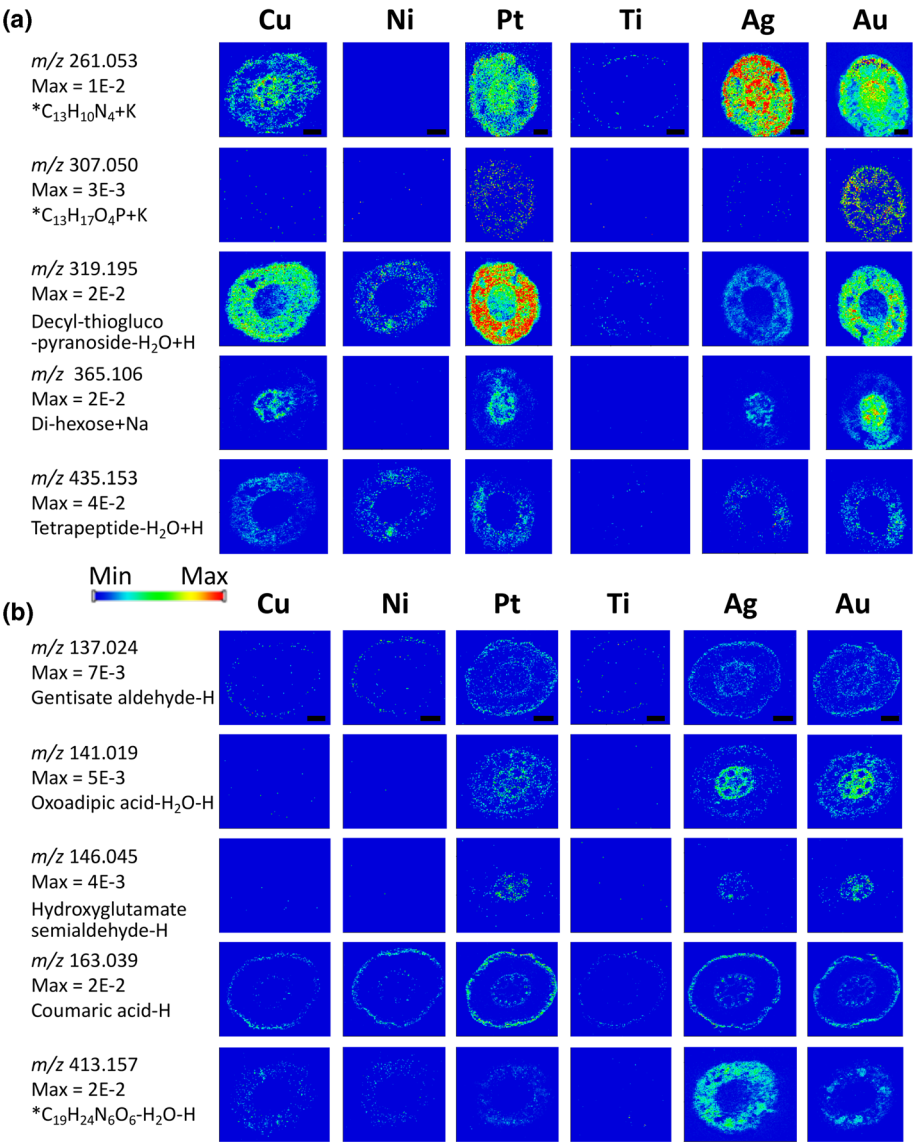


**Figure 4.** Selected maize root images in (**a**) positive ion mode and (**b**) negative ion mode for the metal matrices. Images are normalized to the TIC and each individual metabolite is set to the same maximum and minimum value for all six matrices. The maximum value is listed for each metabolite. Scale bar = 100 μm. Identifications also listed in Supplemental Table 5

Therefore, for lower mass range metabolites, and particularly sugar-containing species, 10 s Au seems to be optimal. Despite this, for relatively larger metabolites such as TAGs on-tissue, thicker coatings of Au may be optimal as noted by Dufresne et al. [14], although 10 s Au does provide useful TAG images in maize seeds (Fig. 5).

## *Maize Root Imaging*

As we found sputter coating of metals to be efficient for LDI analysis of most metabolites, we applied the metal matrices for imaging of maize root cross-sections. The optimal sputtering times from the standard analyses were used in all imaging studies. Consecutive B73 inbred maize root sections were analyzed using all six metal matrices in both ion modes at 10 μm high-spatial resolution. Figure 3a shows overlays of false color images consisting of three representative metabolites for each matrix. These metabolites were chosen from among the most intense ion signals with each matrix that highlight interesting metabolite localizations. Figure 3b shows the morphology of a maize root cross-section with structural features listed. Averaged spectra from on-tissue areas of each maize cross-section can be found in Supplemental Figure 3. Many of these compounds were identified through MS/MS, or at least their molecular formulae were determined from the accurate mass, as summarized in Supplemental Table 5.

Visually, it is readily apparent that Ti is not an effective matrix in either positive or negative ion modes. This can largely be attributed to the low overall signal obtained using Ti as a matrix, which can be also seen in Supplemental Figure 3F and

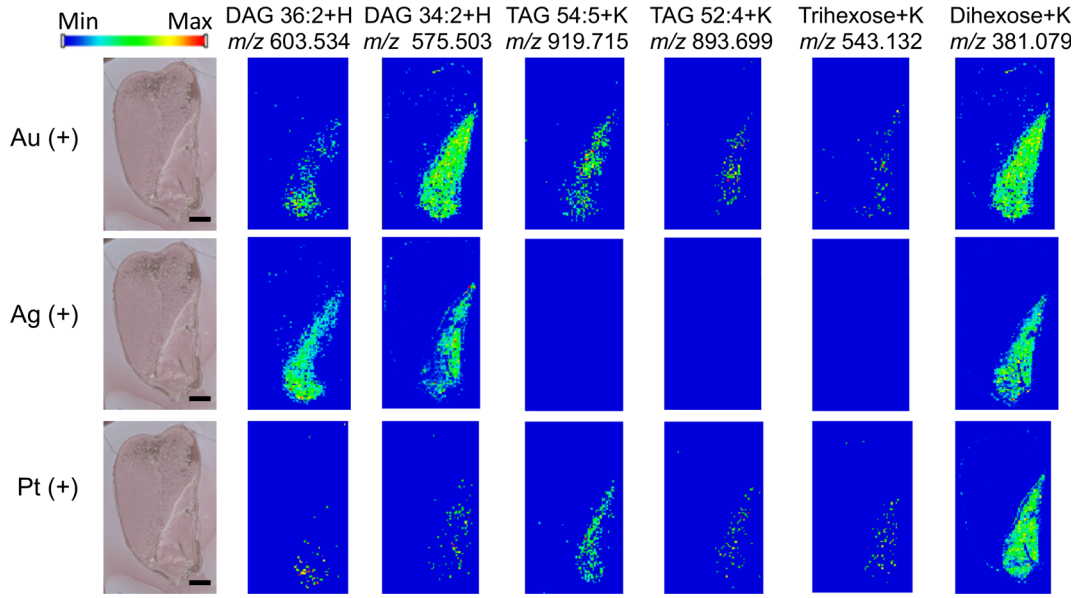


**Figure 5.** Neutral lipids and some sugars in maize seeds with Au, Ag, and Pt metal matrices in positive ion mode. DAG diacylglycerol, TAG triacylglycerol. Scale bar = 1.5 mm

3L. Although some real metabolite signals are present and images can be generated, in comparison to other matrices, Ti is the worst performer. Ni, although better than Ti, also displays low ion signals (Supplemental Figure 3E and 3K) as well as lower quality images than Ag, Au, or Pt. Additionally, metabolites that could be ionized with Ti and Ni were more effectively ionized with other metal matrices. The remaining metal matrices studied, Au, Ag, Pt, and Cu, all produced higher quality images (Fig. 3a) and also useful and informative spectra (Supplemental Figure 3A–D, G–J). The metal matrices in this study do not produce evident matrix peaks, except Ag, which produces silver cluster ions in positive mode, but with less than 15% relative abundance.

In positive mode, metabolites that are mainly localized to the cortex include *m/z* 319.195 (Ag, decyl-thioglucopyranoside), 435.153 (Cu, AspPheAspGly or AspPheGlyAsp), 130.933 (Ni, unknown), and 347.189 (Ni, $C_{21}H_{28}N_2$) (Fig. 3a). Some metabolites found only in the stele include *m/z* 365.107 (Ag) and 381.080 (Cu), which are a sodiated and potassiated disaccharide, respectively. Some metabolites are found to be localized to the xylem, such as *m/z* 140.891 (Ag, unknown) and 212. 852 (Pt, unknown). Additionally, some metabolites are localized throughout the root tissue, such as *m/z* 201.008 (Pt, unknown), which is localized in the pith and cortex. Negative ion mode also shows many distinct metabolite localizations (Fig. 3a). Especially interesting is *m/z* 163.039 (Pt, coumaric acid or 3-hydroxy cinnamic acid) which is localized to the epidermal cells and the phloem. Also localized primarily in the epidermal cells is *m/z* 194.045 (Ag, $C_9H_9NO_4$). Similarly to positive mode, some species are localized to only the cortex, such as *m/z* 413.157 (Ag, $C_{19}H_{24}N_6O_6$), 531.209 (Pt, $C_{25}H_{32}N_4O_9$), and 122.024 (Cu, nicotinic acid or picolinic acid). Other metabolites are localized to the cortex and phloem, *m/z* 318.982 (Au, unknown) and 163.112 (Cu, jasmone), and other compounds are primarily found in the pith, such as *m/z* 141.019 (Au, 2-oxoadipic acid), 113.024 (Ag, glutaric acid), and 146.045 (Pt, hydroxyglutamate semialdehyde).

Selected compounds from Fig. 3 are compared with all six metal matrices in positive mode (Fig. 4a) and negative mode (Fig. 4b). Images are normalized to the total ion count and the same maximum and minimum values are used for a particular metabolite across all matrices. Similar efficiency patterns across the metal matrices are seen with all detected adducts. Tentative identifications for these metabolites are in Supplemental Table 5. It is readily apparent that Au, Ag, and Pt are the top performing matrices in both ion modes; however, Cu performs comparably well in positive mode, but is less effective in negative mode. In positive mode, every matrix, except for Ti, was almost equally effective for *m/z* 435.153, which was tentatively identified as a tetrapeptide AspPheAspGly or AspPheGlyAsp. Pt was the most efficient matrix for *m/z* 319.195 (decyl-thioglucopyranoside); however, this metabolite can also be adequately visualized with other metal matrices. Ag was the most effective matrix for *m/z* 261.053 ($C_{13}H_{10}N_4$), although again this metabolite could be detected with other matrices. In negative mode, Ag is the top performing matrix for *m/z* 413.157 ($C_{19}H_{24}N_6O_6$), although this metabolite can be visualized to some extent with the other metal matrix, except for Ti. Most of the metabolites could be visualized equally well with Ag, Au, and Pt in negative mode. Ti is the most ineffective matrix in both positive and negative ion modes.

## *Maize Seed Imaging*

In the standard analysis, we have shown neutral lipids such as DAGs and TAGs can be effectively analyzed with Ag, Au, Cu, and Pt, although analysis of phospholipid species proved unsuccessful in both ion modes with all six metal matrices. The

neutral lipids, however, are present with very low abundance in roots, and were not imaged in the previous section. We have previously shown maize seeds contain various classes of lipid species, including several phospholipids and neutral lipids [22, 23]. In order to demonstrate the visualization of neutral lipid species using metal matrices, maize seed cross-sections were imaged in Fig. 5 using sputter-coated Au, Ag, and Pt. Although images for the potassiated species are shown in the figure, sodiated species are also detected and show analogous distributions. It should be noted that maize seeds have a high potassium content throughout the tissues, and these images are consistent with our previous work with DHB [22] and $Fe_3O_4$ nanoparticles [24]. The summed mass spectra are also compared in Supplemental Figure 4. Au performed the best for visualizing neutral lipids, although Ag is comparable for DAG species and Pt shows some TAG species. As expected from the standard analysis (Fig. 1), Ag performed very poorly for TAG species, giving almost no signal. The reason Ag is effective for DAG species, but not TAGs in this study is currently unknown. However, Lauzon et al. was able to successfully image TAG species in fingerprints using a thicker Ag layer of ~ 14 nm with a FTICR instrument [25]. Ag was also ineffective for higher sugar species, such as trihexose, but Au and Pt could visualize this metabolite (Fig. 5). All three metals were effective for a disaccharide, however (Figs. 1 and 4a). As with the standard analysis, phospholipid species could not be imaged with any of the metal matrices in either ion mode, which is a major limitation of sputter-coated metals as LDI matrices. Ozawa et al., however, was able to detect phosphocholine species using a combination of sputtered Pt and DHB [16].

## Conclusions

We have shown various metals can be sputter coated and used as a matrix for LDI-MS. Overall, however, noble metal NPs (i.e., Au, Ag, and Pt) were found to be very effective for a broader range of compounds, compared to the other metals studied (Cu, Ni, Ti). Sputter-coated metals present distinct advantages as LDI matrices in that (1) there is little to no matrix background and (2) they can be uniformly deposited. Therefore, sputter-coated metal matrices are extremely useful for high-spatial resolution mass spectrometry imaging of small molecules. In this work, we successfully applied metal sputter coating to the imaging of maize root cross-sections at 10 μm spatial resolution which allowed many distinct small molecule metabolite localizations to be revealed. This study also determined that the optimal nanoparticle deposition time for the six metal matrices was Ag 5 s, Au 10 s, Pt 10 s, Ni 30 s, and Ti 30 s in both ion modes, and Cu 5 s for negative and 60 s for positive mode. It should be noted that the presented optimal deposition times/thicknesses could vary depending on instrument setup, metabolites of interest, or tissue type; however, in our experiments, the optimal metal thicknesses are all relatively thin and increased thicknesses result in decreased signal intensities and poorer quality images.

Importantly, in comparison to two common organic matrices (DHB and DAN), metal sputter coating is more effective in both positive and negative ion modes for a broad range of small metabolites, almost independently of the particular kind of analytes according to our screening results with a small set of standards. However, for the on-tissue analysis of maize root cross-sections, some metabolites have shown moderate specificity for a particular metal matrix. As the standard analyte comparison encompassed only a small number of different classes of compounds, it is possible that there may be some selectivity with metal matrices with untested compound classes. Nevertheless, one possible explanation for the general lack of matrix-dependent analyte specificity and high LDI efficiency of noble metals might be the non-reactivity of noble metals. In contrast, however, the transition metals may react with the analytes or form oxides with trace oxygen present during the sputter process, thus limiting their effectiveness. It is not clear why all six metals tested were particularly ineffective for the analysis of phospholipid species, while noble metals, especially Au, were successful for neutral lipid analysis.

## Acknowledgements

This work was partially funded by the United States Department of Agriculture-National Institute of Food and Agriculture (USDA-NIFA).

## References

1. Shrivas, K., Hayasaka, T., Sugiura, Y., Setou, M.: Method for simultaneous imaging of endogenous low molecular weight metabolites in mouse brain using TiO2 nanoparticles in nanoparticle-assisted laser desorption/ionization-imaging mass spectrometry. Anal. Chem. **83**, 7283–7289 (2011)
2. Lu, M., Yang, X., Yang, Y., Qin, P., Wu, X., Cai, Z.: Nanomaterials as assisted matrix of laser desorption/ionization time-of-flight mass spectrometry for the analysis of small molecules. Nano. **7**, 87 (2017)
3. Cha, S., Yeung, E.S.: Colloidal graphite-assisted laser desorption/ionization mass spectrometry and MSn of small molecules. 1. Imaging of cerebrosides directly from rat brain tissue. Anal. Chem. **79**, 2373–2385 (2007)
4. Wang, J., Liu, Q., Liang, Y., Jiang, G.: Recent progress in application of carbon nanomaterials in laser desorption/ionization mass spectrometry. Anal. Bioanal. Chem. **408**, 2861–2873 (2016)
5. Yagnik, G.B., Hansen, R.L., Korte, A.R., Reichert, M.D., Vela, J., Lee, Y.J.: Large scale nanoparticle screening for small molecule analysis in laser desorption ionization mass spectrometry. Anal. Chem. **88**, 8926–8930 (2016)
6. Zhu, Z.-J., Tang, R., Yeh, Y.-C., Miranda, O.R., Rotello, V.M., Vachet, R.W.: Determination of the intracellular stability of gold nanoparticle monolayers using mass spectrometry. Anal. Chem. **84**, 4321–4326 (2012)
7. Tang, J., Liu, Y., Qi, D., Yao, G., Deng, C., Zhang, X.: On-plate-selective enrichment of glycopeptides using boronic acid-modified gold nanoparticles for direct MALDI-QIT-TOF MS analysis. Proteomics. **9**, 5046–5055 (2009)
8. Liang, Q., Sherwood, J., Macher, T., Wilson, J.M., Bao, Y., Cassady, C.J.: Citric acid capped iron oxide nanoparticles as an effective MALDI matrix for polymers. J. Am. Soc. Mass Spectrom. **28**, 409–418 (2017)
9. Amendola, V., Litti, L., Meneghetti, M.: LDI-MS assisted by chemical-free gold nanoparticles: enhanced sensitivity and reduced background in the low-mass region. Anal. Chem. **85**, 11747–11754 (2013)

10. Taira, S., Sugiura, Y., Moritake, S., Shimma, S., Ichiyanagi, Y., Setou, M.: Nanoparticle-assisted laser desorption/ionization based mass imaging with cellular resolution. Anal. Chem. **80**, 4761–4766 (2008)
11. Liang, Q., Macher, T., Xu, Y., Bao, Y., Cassady, C.J.: MALDI MS in-source decay of glycans using a glutathione-capped iron oxide nanoparticle matrix. Anal. Chem. **86**, 8496–8503 (2014)
12. Tang, H.-W., Wong, M.Y.-M., Lam, W., Cheng, Y.-C., Che, C.-M., Ng, K.-M.: Molecular histology analysis by matrix-assisted laser desorption/ionization imaging mass spectrometry using gold nanoparticles as matrix. Rapid Commun. Mass Spectrom. **25**, 3690–3696 (2011)
13. Dufresne, M., Thomas, A., Breault-Turcot, J., Masson, J.-F., Chaurand, P.: Silver-assisted laser desorption ionization for high spatial resolution imaging mass spectrometry of olefins from thin tissue sections. Anal. Chem. **85**, 3318–3324 (2013)
14. Dufresne, M., Masson, J.-F., Chaurand, P.: Sodium-doped gold-assisted laser desorption ionization for enhanced imaging mass spectrometry of triacylglycerols from thin tissue sections. Anal. Chem. **88**, 6018–6025 (2016)
15. Xu, L., Kliman, M., Forsythe, J.G., Korade, Z., Hmelo, A.B., Porter, N.A., McLean, J.A.: Profiling and imaging ion mobility-mass spectrometry analysis of cholesterol and 7-dehydrocholesterol in cells via sputtered silver MALDI. J. Am. Soc. Mass Spectrom. **26**, 924–933 (2015)
16. Ozawa, T., Osaka, I., Ihozaki, T., Hamada, S., Kuroda, Y., Murakami, T., Miyazato, A., Kawasaki, H., Arakawa, R.: Simultaneous detection of phosphatidylcholines and glycerolipids using matrix-enhanced surface-assisted laser desorption/ionization-mass spectrometry with sputter-deposited platinum film. J. Mass Spectrom. **50**, 1264–1269 (2015)
17. Feenstra, A.D., Dueñas, M.E., Lee, Y.J.: Five micron high resolution MALDI mass spectrometry imaging with simple, interchangeable, multi-resolution optical system. J. Am. Soc. Mass Spectrom. **28**, 434–442 (2017)
18. Guijas, C., Montenegro-Burke, J.R., Domingo-Almenara, X., Palermo, A., Warth, B., Hermann, G., Koellensperger, G., Huan, T., Uritboonthai, W., Aisporna, A.E., Wolan, D.W., Spilker, M.E., Benton, H.P., Siuzdak, G.: METLIN: a technology platform for identifying knowns and unknowns. Anal. Chem. **90**, 3156–3164 (2018)
19. Allen, F., Pon, A., Wilson, M., Greiner, R., Wishart, D.: CFM-ID: a web server for annotation, spectrum prediction and metabolite identification from tandem mass spectra. Nucleic Acids Res. **42**, W94–W99 (2014)
20. Li, J., Liu, J., Liu, Z., Tan, Y., Liu, X., Wang, F.: Water-soluble Au nanoclusters for multiplexed mass spectrometry imaging. Chem. Commun. **53**, 12688–12691 (2017)
21. Klein, A.T., Yagnik, G.B., Hohenstein, J.D., Ji, Z., Zi, J., Reichert, M.D., MacIntosh, G.C., Yang, B., Peters, R.J., Vela, J., Lee, Y.J.: Investigation of the chemical interface in the soybean–aphid and rice–bacteria interactions using MALDI-mass spectrometry imaging. Anal. Chem. **87**, 5294–5301 (2015)
22. Feenstra, A.D., Alexander, L.E., Song, Z., Korte, A.R., Yandeau-Nelson, M., Nikolau, B.J., Lee, Y.-J.: Spatial mapping and profiling of metabolite distributions during germination. Plant Physiol. **174**, 2532–2548 (2017)
23. Dueñas, M.E., Carlucci, L., Lee, Y.J.: Matrix recrystallization for MALDI-MS imaging of maize lipids at high-spatial resolution. J. Am. Soc. Mass Spectrom. **27**, 1575–1578 (2016)
24. Feenstra, A.D., O'Neill, K.C., Yagnik, G.B., Lee, Y.J.: Organic-inorganic binary mixture matrix for comprehensive laser-desorption ionization mass spectrometric analysis and imaging of medium-size molecules including phospholipids, glycerolipids, and oligosaccharides. RSC Adv. **6**, 99260–99268 (2016)
25. Lauzon, N., Dufresne, M., Chauhan, V., Chaurand, P.: Development of laser desorption imaging mass spectrometry methods to investigate the molecular composition of latent fingermarks. J. Am. Soc. Mass Spectrom. **26**, 878–886 (2015)